Enhancement in interface robustness regarding thermal oxidation in nanostructured Al 2 O 3 deposited on 4 H -SiC

S. A. Corrêa, G. G. Marmitt, N. M. Bom, A. T. da Rosa, F. C. Stedile, C. Radtke, G. V. Soares, I. J. R. Baumvol, C. Krug, and A. L. Gobbi

---

Articles you may be interested in

Growth of silicon quantum dots by oxidation of the silicon nanocrystals embedded within silicon carbide matrix
AIP Advances **4**, 107106 (2014); 10.1063/1.4897378

Electrical and spectroscopic comparison of HfO 2 / Si interfaces on nitrided and un-nitrided Si(100)
J. Appl. Phys. **91**, 4353 (2002); 10.1063/1.1455155

Effects of nitridation and annealing on interface properties of thermally oxidized SiO 2 / SiC metal–oxide–semiconductor system
Appl. Phys. Lett. **76**, 3744 (2000); 10.1063/1.126769

Wet oxidation of amorphous Si 0.67 Ge 0.25 C 0.08 grown on (100) Si substrates
J. Appl. Phys. **83**, 2835 (1998); 10.1063/1.367044

Structure and composition of oxidized aluminum on NiO(100)
J. Vac. Sci. Technol. A **15**, 532 (1997); 10.1116/1.580679

Enhancement in interface robustness regarding thermal oxidation in nanostructured Al$_2$O$_3$ deposited on 4H-SiC

S. A. Corrêa,[1] G. G. Marmitt,[1] N. M. Bom,[1] A. T. da Rosa,[1] F. C. Stedile,[1] C. Radtke,[1,a)]
G. V. Soares,[2] I. J. R. Baumvol,[2,3] C. Krug,[3] and A. L. Gobbi[4]

[1]*Instituto de Química, UFRGS, Porto Alegre, Rio Grande do Sul 91509-900, Brazil*
[2]*Universidade de Caxias do Sul, Caxias do Sul, Rio Grande do Sul 95070-560, Brazil*
[3]*Instituto de Física, UFRGS, Porto Alegre, Rio Grande do Sul 91509-900, Brazil*
[4]*Laboratório Nacional de Luz Síncrotron, Campinas, São Paulo 13083-100, Brazil*

Experimental evidences of enhanced stability of Al$_2$O$_3$/SiC structures following thermal annealing are presented. 5- and 40-nm-thick Al$_2$O$_3$ films evaporated on the Si- and C-terminated faces of 4H-SiC were annealed up to 1000 °C in different atmospheres, leading to crystallization and densification of Al$_2$O$_3$, with an increase in the band gap. Exposure to O$_2$ at high temperatures produced SiO$_2$ and AlSi$_x$O$_y$ at the Al$_2$O$_3$/SiC interface, with less silicate on the Si-terminated face. Annealing in N$_2$ before exposure to O$_2$ hindered oxygen diffusion and exchange, leading to more stable thin film structures from the point of view of atomic transport. © *2009 American Institute of Physics*. [DOI: 10.1063/1.3195702]

Significant research effort is being made to exploit the excellent properties of silicon carbide (SiC) for power electronics. With a band gap approximately three times larger than that of silicon (Si), SiC also presents higher breakdown electric field and thermal conductivity.[1] Among wide-bandgap materials, only SiC can be thermally oxidized to produce silicon oxide (SiO$_2$) as in the case of Si. This has raised expectations regarding the realization of SiC-based metal-oxide-semiconductor field effect transistors (MOS-FETs). However, channel mobilities in actual devices are only a fraction (approximately 1%) of the bulk carrier mobility in SiC. The imperfect nature of the thermal SiO$_2$/SiC interface is considered to be the main source of channel resistance in SiC MOSFETs.[2] Recently, combined transmission electron microscopy and electron energy loss spectroscopy analyses[3] revealed that thermal oxidation also involves structural degradation of the top few atomic layers of the SiC substrate.

Deposition of a suitable material to act as a gate dielectric on SiC should eliminate the issues associated with thermal oxidation. Aluminum oxide (Al$_2$O$_3$) is attractive as dielectric because it simultaneously presents a significant dielectric constant ($k \approx 9$) and large band offsets[4] to 4H-SiC in comparison to common high-k materials. There are open questions, however, with respect to both fabrication and reliability of Al$_2$O$_3$ as the gate dielectric for SiC devices submitted to the extreme conditions intrinsic to power electronics.

An interfacial Si suboxide layer between Al$_2$O$_3$ prepared by atomic layer deposition (ALD) and the Si-terminated face of 4H-SiC was evidenced by x-ray photoelectron spectroscopy (XPS). The interlayer thickness increased after annealing at 1000 °C in Ar, which also triggered Si diffusion into the dielectric layer as evidenced by secondary ion mass spectrometry.[5] The thickness of a SiO$_2$ interlayer has significant impact on channel mobility for Al$_2$O$_3$/4H-SiC MOSFETs.[6] Thus, controlling the transport of oxygen

through Al$_2$O$_3$ is mandatory. Besides the formation of an interlayer and compositional changes in the dielectric, thermal annealing also induces structural modifications in Al$_2$O$_3$, as shown by Jakschik *et al.*[7] In particular, an increase in the dielectric constant was observed accompanying crystallization and densification.

In this scenario, we investigated Al$_2$O$_3$/4H-SiC structures with respect to atomic transport and interface modification induced by thermal annealing in O$_2$ or N$_2$. Al$_2$O$_3$ films were deposited on both (0001) (Si-face) and (000$\underline{1}$) (C-face) of 4H-SiC to investigate the influence of substrate polarity on interface formation and stability. Oxygen incorporation was detected using O$_2$ enriched in ^{18}O, whose natural abundance is 0.2%. That enabled us to use nuclear reaction analysis and distinguish oxygen originally in the Al$_2$O$_3$ film from that incorporated during annealing. All results were compared with those of counterpart Al$_2$O$_3$/Si samples.

4H-SiC polished on both (0001) and (000$\underline{1}$) faces and Si(001) substrates were cleaned in a mixture of H$_2$SO$_4$ and H$_2$O$_2$ followed by the RCA process. After etching in a 5% HF aqueous solution for 1 min, samples were rinsed in deionized water for 30 s and loaded in the deposition chamber. Al$_2$O$_3$ films were deposited from an alumina source by electron beam physical vapor deposition, which is not aggressive to the substrate (i.e., minimizes damage) and is free of intrinsic contaminants such as carbon and hydrogen, typical of chemical methods. Deposition parameters were adjusted in order to produce stoichiometric Al$_2$O$_3$ films as determined by Rutherford backscattering spectrometry. XPS was performed in an Omicron SPHERA station using Mg $K\alpha$ radiation. Data fitting was performed using a branching ratio $2p_{1/2}/2p_{3/2}$ of 0.5 (the statistical ratio) and a spin-orbit splitting of 0.6 eV. The samples characterized by XPS had 5-nm-thick Al$_2$O$_3$ layers, while 40-nm-thick films were used for x-ray diffraction (XRD) and reflectivity and nuclear reaction analysis. X-ray reflectivity (XRR) analyses were performed in a Shimadzu XRD 6000 equipment using Cu $K\alpha$ radiation ($\lambda = 1.5418$ Å) and scanning in 0.02° steps. Thermal processing was performed in a resistively heated quartz tube
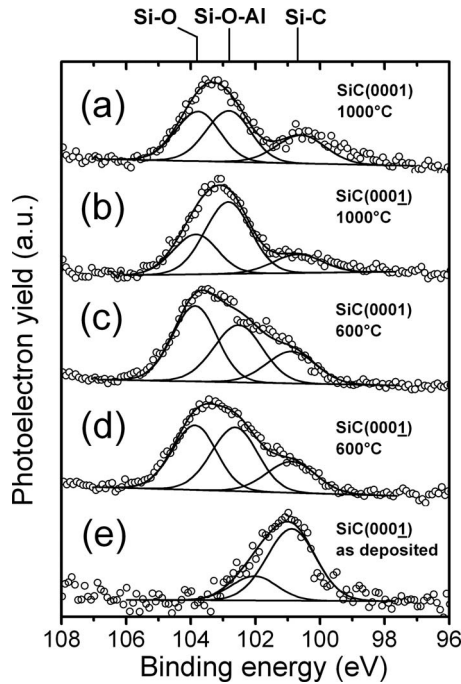
a)Electronic mail: claudio@iq.ufrgs.br.

FIG. 1. Si 2*p* regions of XPS spectra corresponding to samples prepared by annealing in 100 mbar of $^{18}O_2$ for 1 h at 1000 °C [parts (a) and (b)] and 600 °C [parts (c) and (d)] of Al_2O_3 (5 nm) films deposited on the Si [parts (a) and (c)] and C faces [parts (b) and (d)] of 4*H*-SiC. The spectrum obtained from the as-deposited sample prepared on the C face of 4*H*-SiC is also shown [part (e)]. Points represent experimental data. Solid curves correspond to fitting components, background, and their sum. The energy position of components assigned to silicon oxide, $AlSi_xO_y$, and silicon carbide are indicated. a.u. stands for arbitrary units.

FIG. 2. Experimental excitation curves of the $^{18}O(p, \alpha)^{15}N$ nuclear reaction. Al_2O_3 (40 nm)/SiC structures annealed in (top) 100 mbar of $^{18}O_2$ for 1 h at 600 °C (solid circles), 900 °C (solid squares), and 1000 °C (open triangles) and (bottom) 100 mbar of N_2 for 1 h at 900 °C (solid squares) and 1000 °C (open triangles) followed by an oxidation step in 100 mbar of $^{18}O_2$ for 1h at 900 °C. Sketches of the sample processing route are shown at the top of the respective figures. The crystallization induced by annealing is represented by a different filling pattern of the Al_2O_3 film in each sketch.

furnace for 1 h under a static pressure of 100 mbar of either N_2 (<1 ppm of H_2O) or O_2 enriched to 97% in the isotope of mass 18 (termed $^{18}O_2$). The depth distribution of ^{18}O in annealed samples was determined by nuclear reaction profiling using the resonance at 151 keV in the cross-section curve of the $^{18}O(p, \alpha)^{15}N$ nuclear reaction.[8]

Figure 1 shows Si 2*p* XPS spectra for 5-nm-thick Al_2O_3 films on SiC before or after annealing in O_2 at 600 or 1000 °C. We found no significant evidence of an interlayer between Al_2O_3 and SiC substrates in as-deposited samples. A Si substrate counterpart, on the other hand, showed aluminum silicate ($AlSi_xO_y$). The formation of such a compound was also observed with Al_2O_3/Si structures prepared by chemical vapor deposition at 400 °C.[9] This observation should be related to the lower reactivity of SiC when compared to Si. In Fig. 1 three components can be distinguished in the spectra. We assign them to silicon oxide, $AlSi_xO_y$, and the silicon carbide substrate.

Annealing in O_2 affected the Si 2*p* spectrum of all samples as compared to as-deposited ones. Al 2*p* and O 1*s* spectra, on the other hand, remained unchanged. Interface modification took place at 600 °C where, based only on intrinsic carrier concentration, SiC devices can operate theoretically. The degree of modification depends on annealing temperature and substrate polarity. At fixed temperature, $AlSi_xO_y$ is more abundant in the C-faced sample (as determined by comparing the components' areas) while for a given substrate termination, the higher the annealing temperature, the higher the relative amount of silicate. That is, SiO_2 formation is hindered at the highest annealing temperature (similar results were obtained on Si substrate, not shown
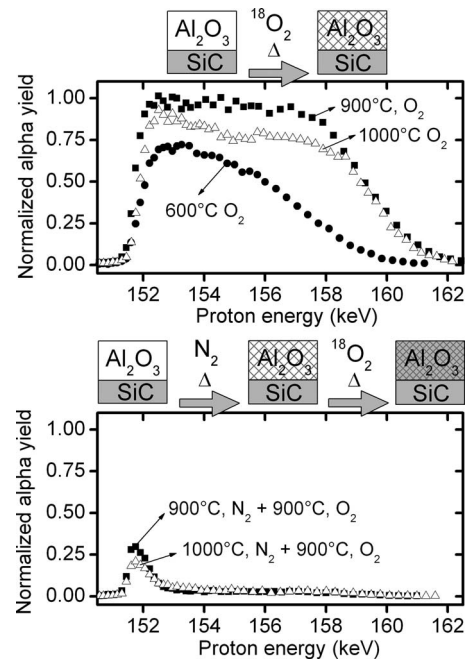
here). According to the data discussed below, this observation is at least partially due to crystallization of Al_2O_3.

$AlSi_xO_y$ formation can be explained by chemical reaction between Al_2O_3 and SiC. SiO_2 formation would be likely due to reduction in Al_2O_3 by SiC or reaction between the substrate and oxygen diffusing from the gas phase. As XPS data only show Al in the fully oxidized state, experimental evidence favors the latter hypothesis. Our observation that $AlSi_xO_y$ is more abundant in the C-terminated face of SiC can be explained by faster kinetics in the reaction of SiC with Al_2O_3, as observed for the reaction with oxygen in thermal oxidation.[10] As for the fact that less SiO_2 forms at high annealing temperature, additional data discussed below indicate that a bulk transformation in Al_2O_3 limits the supply of oxygen from the gas phase (i.e., diffusion is hindered).

Figure 2 shows nuclear reaction data regarding ^{18}O in 40-nm-thick Al_2O_3 films annealed at the indicated temperatures. Alpha particle yield in the figure is proportional to ^{18}O concentration; depth in the sample scales with proton energy. The curves shown correspond to the actual concentration versus depth information convoluted with instrumental and proton energy loss functions. According to Fig. 2, processing at 600 °C leads to a relatively shallow distribution of ^{18}O in Al_2O_3 (i.e., the interface with SiC is barely reached); the maximum concentration of ^{18}O occurs at the sample surface. Annealing at 900 °C produces a constant distribution of ^{18}O in Al_2O_3 that corresponds to 1.4 times the peak concentration observed at 600 °C. Data taken after annealing at 1000 °C indicate a bulk concentration of ^{18}O that is intermediate between those seen at 600 and 900 °C. This result contrasts with the observation[11] that oxygen incorporation and ex-
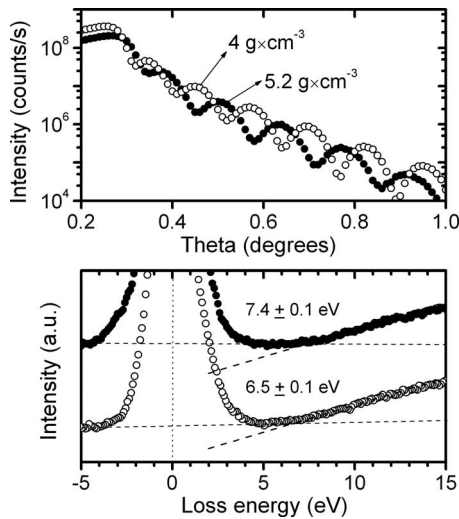
FIG. 3. (Top) XRR experimental data obtained from Al_2O_3 (40 nm)/4H-SiC(0001) structures as-deposited (open symbols) and annealed in 100 mbar of $^{18}O_2$ for 1 h at 1000 °C (solid symbols). Al_2O_3 film densities obtained from these data are listed. (Bottom) Energy loss spectra of O 1s photoelectrons of the same samples. The curves are offset along the intensity axis for clarity. The band gap was determined by linear extrapolation as shown by the dashed lines. a.u. stands for arbitrary units.

change in Al_2O_3 films deposited by ALD on Si tends to increase with annealing temperature.

Aiming at clarifying the observation above, two samples were annealed sequentially for 1 h in 100 mbar of N_2 followed by $^{18}O_2$. As shown in Fig. 2, the annealing step in inert gas significantly reduced the amount of ^{18}O incorporated to the oxide film. In addition, ^{18}O became essentially confined to the sample surface. This result scaled with annealing temperature in N_2: thermal treatment at 900 °C followed by $^{18}O_2$ at 900 °C resulted in more ^{18}O incorporated to the sample surface than the sample annealed in N_2 at 1000 °C following the same oxidation step. XRD showed a signal near $2\theta=67.5°$ (Cu $K\alpha$ radiation) that was attributed to Al_2O_3 which intensity increased with increasing annealing temperature. This indicates that, despite grain boundaries, crystallized Al_2O_3 is more robust regarding incorporation of oxygen. Our understanding is that $AlSi_xO_y$ formation, Al_2O_3 crystallization, and ^{18}O incorporation occur simultaneously, the latter two being competitive processes to a certain extent. From Fig. 2 (top), for annealing at 900 °C the kinetics is such that ^{18}O incorporation is at maximum. At 1000 °C, crystallization is accelerated relative to oxygen diffusion and by the time that ^{18}O reaches the subsurface region of Al_2O_3 the number of reaction sites has been reduced. The crystallization process was accompanied by film densification, as seen in Ref. 7.

XRR measurements (Fig. 3) indicated a reduction of approximately 25% in the Al_2O_3 film thickness after annealing

at 1000 °C. Finally, the band gap extracted from the O 1s XPS loss feature was seen to increase from 6.5 eV in as-deposited to 7.4 eV in annealed samples. These values were obtained from the energy difference between the O 1s photoelectron peak and the onset of the plasmon loss, which is a good approximation to the band gap energy.[12] In Fig. 3, the comparison of O 1s loss spectra is made between an as-deposited Al_2O_3 (40 nm)/SiC sample and the same structure after annealing in $^{18}O_2$ at 1000 °C. Similar loss spectra were observed for all annealed samples. This significant increase should be related to the elimination of band-tail states accompanying oxide crystallization.

In summary, we investigated oxygen transport in Al_2O_3 and thermally driven chemical reactions in the Al_2O_3/SiC interface region. Thermal annealing in the presence of O_2 led to the formation of $AlSi_xO_y$ and SiO_2, with more silicate observed on the C-terminated face of 4H-SiC. Differences such as this are significant regarding the choice of SiC polytype and face for device fabrication. Exposure to high temperatures promoted crystallization and densification of Al_2O_3. When performed in N_2, this annealing significantly lowered the penetration of oxygen in the film. An engineered thermal annealing step that stabilizes Al_2O_3 with respect to oxygen transport without compromising the Al_2O_3/SiC interface with $AlSi_xO_y$ formation might improve the prospects of this oxide-wide band gap semiconductor combination for power electronics.

[1]R. Singh, Microelectron. Reliab. **46**, 713 (2006).
[2]S. Dhar, S. R. Wang, J. R. Williams, S. T. Pantelides, and L. C. Feldman, MRS Bull. **30**, 288 (2005).
[3]T. Zheleva, A. Lelis, G. Duscher, F. Liu, I. Levin, and M. Das, Appl. Phys. Lett. **93**, 022108 (2008).
[4]K. Y. Gao, Th. Seyller, L. Ley, F. Ciobanu, G. Pensl, A. Tadich, J. D. Riley, and R. G. C. Leckey, Appl. Phys. Lett. **83**, 1830 (2003).
[5]M. Avice, S. Diplas, A. Thogersen, J. S. Christensen, U. Grossner, B. G. Svensson, O. Nilsen, H. Fjellvag, and J. F. Watts, Appl. Phys. Lett. **91**, 052907 (2007).
[6]T. Hatayama, S. Hino, N. Miura, T. Oomori, and E. Tokumitsu, IEEE Trans. Electron Devices **55**, 2041 (2008).
[7]S. Jakschik, U. Schroeder, T. Hecht, M. Gutsche, H. Seidl, and J. W. Barthe, Thin Solid Films **425**, 216 (2003).
[8]G. Battistig, G. Amsel, E. d'Artemare, and I. Vickridge, Nucl. Instrum. Methods Phys. Res. B **66**, 1 (1992).
[9]T. M. Klein, D. Niu, W. S. Epling, W. Li, D. M. Maher, C. C. Hobbs, R. I. Hegde, I. J. R. Baumvol, and G. N. Parsons, Appl. Phys. Lett. **75**, 4001 (1999).
[10]I. Vickridge, J. Ganem, Y. Hoshino, and I. Trimaille, J. Phys. D **40**, 6254 (2007).
[11]E. B. O. da Rosa, I. J. R. Baumvol, J. Morais, and R. M. C. de Almeida, Phys. Rev. B **65**, 121303 (2002).
[12]S. Miyazaki, H. Nishimura, M. Fukuda, L. Ley, and J. Ristein, Appl. Surf. Sci. **114**, 585 (1997).